Inorganic Chemistry
Article

Inorg. Chem. **2010**, *49*, 11505–11515 **11505**
DOI: 10.1021/ic101671k

Rhombohedrally Distorted γ-Brasses $Cr_{1-x}Fe_xGa$

Hyunjin Ko,[†] Olivier Gourdon,[‡] Delphine Gout,[‡,§] Eun-Deok Mun,[∥] Srinivasa Thimmaiah,[†] and Gordon J. Miller*,[†]

[†]*Department of Chemistry, Iowa State University and Ames Laboratory, Ames, Iowa 50011-3111, United States,* [‡]*Jülich Center for Neutron Science Outstation at SNS—Oak Ridge National Laboratory, Oak Ridge, Tennessee 37831-6032, United States,* [§]*Oak Ridge National Laboratory, Oak Ridge, Tennessee 37831-6032, United States, and* [∥]*Department of Physics and Astronomy, Iowa State University, Ames, Iowa 50011-3111, United States*

Received August 17, 2010

A series of rhombohedrally distorted γ-brass structures containing a mixture of magnetically active 3d elements, Cr and Fe, $Cr_{1-x}Fe_xGa$, is investigated crystallographically. These structures consist of chains of trans-face-sharing Ga-centered transition metal icosahedra. Neutron powder diffraction specifically on $Cr_{0.5}Fe_{0.5}Ga$, which could be prepared as a single phase material, gave lattice constants (11 K) $a = 12.5172(2)$ Å and $c = 7.8325(2)$ Å and a refined composition of $Cr_{0.502(6)}Fe_{0.498}Ga = Cr_{6.523}Fe_{6.477}Ga_{13}$ and revealed partial ordering of Cr and Fe atoms among three crystallographic sites. Magnetic susceptibility and magnetization studies of $Cr_{0.5}Fe_{0.5}Ga$ showed the onset of magnetic ordering at ca. 25 K. Theoretical calculations suggested both site-energy and bond-energy factors influencing the Cr/Fe distribution. Heteroatomic interactions significantly affect exchange interactions and create low local magnetic moments. Models created to mimic $Cr_{0.5}Fe_{0.5}Ga$ showed ferromagnetic Fe−Fe and antiferromagnetic Cr−Fe interactions, with an overall ferrimagnetic ordering.

Introduction

The relationship between crystal structure and valence electron concentration (vec = number of valence electrons/number of atoms in the chemical formula) in γ-brass phases emphasizes how the electronic structure can influence chemical compositions and atomic arrangements in complex intermetallic compounds. The γ-brasses belong to a class of "Hume−Rothery electron phases," which involve late and post-transition metals and whose structures are controlled by their vec values.[1−3] Specifically, γ-brasses exist for vec values in the range 1.60−1.75 e^-/atom, values which are determined by using only the valence s and p electrons, as found for Cu_5Zn_8, Cu_9Al_4, and Pd_2Zn_{11}.[4] Extensive first-principles calculations on various γ-brass structures identify the existence of a pseudogap at the corresponding Fermi levels.[4,5] Although the structure itself leads to local minima in the electronic density of states (DOS) curves at the Fermi level, the atomic distribution enhances the pseudogap, as in the Cu−Zn system, for example.[6] In the Zn−Pd and Cd−Pd systems, slight variations in chemical composition lead to distinct superstructures of the γ-brass phases.[7−10] The presence of a pseudogap in the DOS curves of two Zn−Pd phases led to a cluster-counting rule that accounts for the periodicity along a single dimension.[7]

In addition to these crystalline intermetallics, many quasicrystals are also called Hume−Rothery electron phases. Ever since Fujiwara's first band structure calculations on the approximants to Al−Mn quasicrystals revealed the existence of a pseudogap at the Fermi level,[11] numerous empirical and *ab initio* studies have shown that the stability of various quasicrystalline phases and their approximants also give a similar outcome in their DOS curves. This so-called Hume−Rothery stabilization rule is important for the stability of many quasicrystals and their approximants. In fact, recent structural and theoretical studies of various γ-brasses reveal close relationships between these crystalline phases and icosahedral quasicrystals.[12,13]

---

*To whom correspondence should be addressed. E-mail: gmiller@iastate.edu.

(1) Mott, N. F.; Jones, H. *The Theory of the Properties of Metals and Alloys*; Dover: Mineola, NY, 1958.

(2) Barrett, C.; Massalski, T. B. *Structure of Metals*; McGraw Hill: New York, 1966.

(3) Massalski, T. B.; Mizutani, U. *Progr. Mater. Sci.* **1978**, *22*, 151.

(4) Mizutani, U.; Asahi, R.; Sato, H.; Takeuchi, T. *Philos. Mag.* **2006**, *86*, 645.

(5) Mizutani, U.; Asahi, R.; Takeuchi, T; Sato, H.; Kontsevoi, O.; Freeman, A. J. *Z. Kristallogr.* **2009**, *224*, 17–20.

(6) Gourdon, O.; Gout, D.; Williams, D. J.; Proffen, T.; Hobbs, S.; Miller, G. J. *Inorg. Chem.* **2007**, *46*, 251.

(7) Gourdon, O.; Izaola, Z.; Elcoro, L.; Petricek, V.; Miller, G. J. *Philos. Mag.* **2006**, *86*, 419–425.

(8) Gourdon, O.; Miller, G. J. *Chem. Mater.* **2006**, *18*, 1848–1856.

(9) Gourdon, O.; Izaola, Z.; Elcoro, L.; Petricék, V.; Miller, G. J. *Inorg. Chem.* **2009**, *48*, 9715–9722.

(10) Schmidt, J. T.; Lee, S.; Fredrickson, D. C.; Conrad, M.; Sun, J.; Harbrecht, B. *Chem.—Eur. J.* **2007**, *13*, 1394.

(11) Fujiwara, J. *Phys. Rev.* **1989**, *B40*, 942.

(12) Berger, R. F.; Lee, S.; Johnson, J.; Nebgen, B.; So, A. C.-Y. *Chem.—Eur. J.* **2008**, *14*, 6627.

(13) Sun, J.; Lee, S.; Lin, J. *Chem. Asian J.* **2007**, *2*, 1204.

As part of an effort to study the properties and electronic structures of icosahedral quasicrystal approximants, we reported on the structural and magnetic characteristics of the series MGa (M = Cr, Mn, Fe),[14,15] which adopts the rhombohedral Cr_5Al_8 structure type.[16,17] In fact, this structure is also a rhombohedral distortion of the cubic γ-brass structure, a distortion which has been attributed to electronic ("band structure") factors.[18] The isostructural series,CrGa−MnGa−FeGa also varies from antiferromagnetic to ferromagnetic behavior, which is important for gaining insight into the relationship between itinerant magnetism and energy band filling.[14,15] In this contribution, we report on the ternary series $Cr_{1-x}Fe_xGa$ with specific focus on the $x \sim 0.50$ case with respect to its magnetic properties and distribution of transition metals. Furthermore, theoretical electronic structures and related computations were evaluated to analyze the relationships among structure, composition, and properties of these phases.

Experimental Section

Synthesis. Eleven compositions in the series of $Cr_{1-x}Fe_xGa$ ($0 \leq x \leq 1$) samples were prepared by heating the pure elements under controlled environments. Prior to these reactions, Cr metal pieces (irregular, 99.99%, Alfa-Aesar) were cleaned in an acidic solution (1:3 ratio by volume of concentrated nitric and hydrochloric acids) for approximately 30 s and rinsed with methanol. Fe metal pieces (irregular, 99.97+%, Alfa-Aesar) were cleaned in an acidic ethanol solution (10:1 ratio by volume of ethanol and concentrated nitric acid) for 2 min and rinsed with methanol, while Ga metal ingots (99.99%, Alfa-Aesar) were used without any pretreatment. To prevent the formation of any oxide phases and to minimize the formation of other impurities, the elements were then individually melted in an arc furnace on a copper hearth under an argon atmosphere. The subsequent surface oxide layer of the ingots was removed by filing. Stoichiometric mixtures of $Cr_{1-x}Fe_xGa$ ($0 \leq x \leq 1$, increments of 0.1, loading errors were less than 0.001% by weight for 3 g samples) were heated in sealed, evacuated silica tubes at 1323 K for 80 h to promote the optimum diffusion of Cr and Fe metals into liquid Ga. After cooling at a rate of 1 K/min to 1123 K, the homogenized sample was annealed at 1123 K for 1 week. Termination of the solid state reaction occurred by turning off the furnace, and the product was allowed to cool naturally to room temperature. Visual inspection and powder X-ray diffraction experiments taken after more than 4 months of product formation revealed the products to be stable against decomposition in both air and moisture at room temperature.

Chemical Analysis. The phase purities of the products were analyzed using energy dispersive spectroscopy (EDS) by a JEOL 840A scanning electron microscope, equipped with an IXRF Systems Iridium X-ray analyzer with a Kevex Quantum thin-window Si(Li) detector for quantitative chemical analysis with Si as the internal standard. Typical data collections utilized a 20 kV accelerating voltage and a 30 nA beam current. No significant oxygen or silicon contamination was observed for all products.

Diffraction Experiments. Phase analysis was performed using powder X-ray diffraction (XRD) at room temperature, and crystal structures were confirmed using single-crystal XRD. Temperature-dependent neutron powder diffraction was carried out specifically on "$Cr_{0.5}Fe_{0.5}Ga$" to obtain the atomic distribution.

Powder XRD. Phase characterizations were performed on several separately prepared samples from each of the products using room-temperature powder XRD using an Enraf-Nonius Guinier camera with Cu Kα radiation (λ = 1.540598 Å) and Si as an internal standard. Patterns were collected for 2θ values ranging from 10° to 95° at increments of 0.02°. Lattice parameters were determined by the Rietveld profile fitting method using the Rietica program for all samples;[19] atomic parameters were refined using the General Structure Analysis System (GSAS) program package[20] for the sample of "$Cr_{0.5}Fe_{0.5}Ga$," which was closest to single phase. Furthermore, to compare with subsequent neutron powder diffraction experiments, temperature-dependent powder XRD measurements were carried out on "$Cr_{0.5}Fe_{0.5}Ga$" for eight different temperatures between ca. 15 and 300 K. All powder diffraction experiments required an exposure time of at least 120 min to obtain peak intensities high enough to be refined because all patterns showed very high background intensities, due to fluorescence problems from the Fe content of the samples.

Single-Crystal XRD. Several irregularly shaped, small crystals with average approximate dimensions of 120 μm^3 were selected from crushed samples of various $Cr_{1-x}Fe_xGa$ products and mounted on glass fibers. Each data set was collected on a Bruker Apex diffractometer at 295(2) K using monochromated Mo Kα radiation (λ = 0.71073 Å) and a detector-to-crystal distance of 5.990 cm. Diffraction data were collected in a hemisphere or full sphere of reciprocal space with 0.3° scans in ω for an exposure time of 10 s per frame up to a maximum 2θ value of 56.55°. The measured intensities were corrected for Lorenz and polarization effects and were further corrected for absorption using the STOE X-SHAPE[21] and X-RED programs.[22] Structure refinements via full-matrix least-squares on F^2 were performed by using the SHELXTL-PLUS programs.[23]

Neutron Powder Diffraction on $Cr_{0.5}Fe_{0.5}Ga$. Due to the nearly indistinguishable X-ray scattering factors between Cr and Fe, neutron powder diffraction experiments were performed on a ca. 5 g powder sample of "$Cr_{0.5}Fe_{0.5}Ga$" to achieve better resolution of the transition metal site occupancies. Indeed, the elastic neutron cross-sections for Cr (1.66×10^{-24} cm^2) and Fe (11.22×10^{-24} cm^2) are significantly different, which allows us to refine site distributions accurately. Time-of-flight (TOF) neutron diffraction data were collected at 11, 30, and 295 K on the neutron powder diffractometer (NPDF) at the Manuel Lujan Neutron Scattering Center of Los Alamos National Laboratory. This instrument is a high-resolution powder diffractometer located at flight path 1, 32 m from the spallation neutron target. The data were collected using the 148°, 119°, 90°, and 46° banks, which cover a d-spacing range from 0.12 to 7.2 Å.

The structures at 11, 30 and 295 K were refined using JANA2006 with a Rietveld profile analysis program[24] using the MnGa structure as the starting structural model. The refinements were performed using the four banks (148°, 119°, 90°, and 46°) simultaneously to obtain unit cell parameters, atomic positions, and equivalent isotropic displacement parameters. Background coefficients, scale factors, isotropic strain terms in the profile function, and sample absorption were also refined for a total of 63 parameters using the centrosymmetric space group $R\bar{3}m$. Alternative refinements were carried out in the space groups $R3m$ and $R\bar{3}$. To elucidate the arrangement and concentration of Cr and

---

(14) Gourdon, O.; Miller, G. J. *J. Solid State Chem.* **2003**, *173*, 137.

(15) Gourdon, O.; Bud'ko, S.; Williams, D.; Miller, G. J. *Inorg. Chem.* **2004**, *43*, 3210.

(16) Bradley, A. J.; Lu, S.-S. *Z. Kristallogr.* **1937**, *96*, 20.

(17) Visser, J. W. *Acta Crystallogr., Sect. B* **1977**, *B33*(316), 1088.

(18) Brandon, J. K.; Pearson, W. B.; Riley, P. W.; Chieh, C.; Stokhuyzen, R. *Acta Crystallogr.* **1977**, *B33*, 1088.

(19) Rietveld, H. M. *J. Appl. Crystallogr.* **1969**, *2*, 65. Hunter, B. A.; Howard, C. J. *Rietica*; Australian Nuclear Science and Technology Organization: Menai, Australia, 2000.

(20) Larson, A. C.; Von Dreele, R. B. *GSAS: General Structure Analysis System*; Los Alamos National Laboratory: Los Alamos, NM, 1985.

(21) *X-SHAPE (2.07): Crystal Optimization for Numerical Absorption Correction*; STOE & Cie.: Darmstadt, Germany, 2005.

(22) *X-RED (1.31): Data Reduction Program*; Stoe & Cie.: Darmstadt, Germany, 2005.

(23) *SHELXTLPlus (6.14)*; Bruker AXS, Inc.: Madison, WI, 2003.

(24) Petricek, V.; Dusek, M.; Palatinus, L. *JANA2006: The crystallographic computing system*; Institute of Physics: Praha, Czech Republic, 2006.

Fe in "$Cr_{0.5}Fe_{0.5}Ga$," the occupancies were also refined, which added three parameters.

Magnetization Measurements. The dc magnetization as a function of temperature from 1.8 to 300 K, and magnetic field, up to 55 kOe, were measured on a Quantum Design (QD) Magnetic Property Measurement System (MPMS). Temperature-dependent magnetization data were collected after the polycrystalline powder samples of "$Cr_{0.5}Fe_{0.5}Ga$" were placed in a gel-capsule fixed in a straw by first measuring zero-field cooled (ZFC) magnetization and then the field-cooled (FC) data.

Electronic Structure Calculations. Theoretical electronic structures of various model structures of $Cr_{1-x}Fe_xGa$ were calculated self-consistently by using the tight-binding, linear muffin-tin-orbital (TB-LMTO) method[25−28] within the atomic sphere approximation (ASA) using the Stuttgart code.[29] Exchange and correlation were treated in a local spin density approximation (LSDA).[30] All relativistic effects except spin−orbit coupling were taken into account using a scalar relativistic approximation.[31] Within the ASA, space is filled by overlapping Wigner−Seitz (WS) atomic spheres. The radii of these WS spheres were obtained by requiring the overlapping potential to be the best possible approximation to the full potential according to an automatic procedure.[32] The WS radii for the atomic sites determined by this procedure are in the ranges 1.465−1.535 Å for Ga sites, 1.461−1.475 Å for Cr, and 1.455−1.481 Å for Fe. The basis set included 4s and 4p orbitals for Ga and 4s, 4p, and 3d orbitals for Cr and Fe. The reciprocal space integrations to determine the self-consistent total energies and charge densities, densities of states (DOS) curves, and crystal orbital Hamilton population (COHP)[33] curves were performed using the tetrahedron method[34] using 65 *k*-points all-model structures in the irreducible wedges of the corresponding Brillouin zones.

Results and Discussion

Phase Identification. Results obtained from EDS, as well as powder and single-crystal XRD, are summarized in Table 1. Most specimens showed multiple phases according to EDS. Throughout the composition range in $Cr_{1-x}Fe_xGa$ from $x = 0.1$ to 0.9, the major phase was identified as the rhombohedral Cr_5Al_8-type structure, and subsequent refinements of diffraction data proceeded well in the centrosymmetric space group $R\overline{3}m$. $Cr_{0.5}Fe_{0.5}Ga$, as loaded, produced an essentially single-phase product according to both EDS and powder XRD measurements. All other samples yielded majority products near the targeted composition. For the range $0.1 \leq x \leq 0.3$, a cubic Cr_3Ga-type structure was indexed, and for the samples with $x = 0.2$ and 0.3, an additional tetragonal $FeGa_3$-type phase was also identified using powder XRD. For loaded compositions with $x \geq 0.8$, a monoclinic Fe_3Ga_4-type phase could be indexed with powder XRD as a secondary phase. Throughout the entire composition range, no other impurity peaks were observed with powder XRD. For the binary specimens, the Fe−Ga preparation yielded a mixture of Fe_3Ga_4, Fe_2Ga, and FeGa; the Cr−Ga preparation produced CrGa, Cr_3Ga, Cr_2Ga, and $CrGa_4$.

Structure Determinations. The structures of rhombohedral $Cr_{1-x}Fe_xGa$ specimens were refined by single crystal XRD; these results are summarized in Tables 1 and 2. At this point, some comments concerning the refinement of site occupancy factors (SOF) in Table 2 is warranted. Because the X-ray scattering powers of Cr and Fe differ by at most 8.3%, the strong correlation between SOF and isotropic temperature displacement parameters makes accurate refinement of the chemical composition of these single crystal specimens challenging when Mo Kα is the incident radiation. The lattice parameters vary monotonically with loaded composition, results which led us to conclude that there is a smooth variation in the Cr/Fe content for the different specimens. To overcome correlation problems during structural refinements, at first we fixed the isotropic displacement parameters to the refined values for the mixed sites and refined the occupancy parameters. In the following step, the occupancies were fixed to these refined values and the displacement parameters were refined. All final cycles of structural refinements were carried out using anisotropic displacement parameters for all atoms. The resulting compositions refined from single crystal X-ray diffraction analyses listed in Table 2 are consistent with those from EDS. We have included estimated uncertainties in the total refined compositions listed in Table 2, but as the final refinement cycle did not include varying the site occupancy factors, we do not list uncertainties for these values (see discussion above). Rather, such uncertainties will occur in the refined displacement parameters. As the Fe content increases, there are monotonic decreases in the unit cell parameters (*a* and *c* axes lengths) as well as unit cell volumes, trends which are consistent with the size relationship between Cr and Fe atoms using their 12-coordinate metallic radii ($r_{Cr} = 1.26$ Å and $r_{Fe} = 1.25$ Å).[38] In addition, the unit cell volume for MnGa is ca. 3% larger than the volume for nearly isoelectronic $Cr_{0.5}Fe_{0.5}Ga$, sample **5**, an effect that can be attributed to possibly different magnetic ground states.

Figure 1 illustrates views of a representative $Cr_{1-x}Fe_xGa$ structure both parallel and perpendicular to the *c* axis. These views are compared with related views of the cubic γ-brass structure, views that are parallel and perpendicular to the [111] direction of the cubic cell. On the basis of the centrosymmetric space group $R\overline{3}m$, the Cr_5Al_8 structure type contains six atoms in the asymmetric unit:[16,17] three sites are occupied by Ga; three sites are occupied by nonstatistical mixtures of Cr and Fe atoms. The rhombohedral structures of $Cr_{1-x}Fe_xGa$ are built of chains of face-sharing, atom-centered icosahedra along the *c* axis. There are two types of icosahedra: (i) Ga-centered, $(Cr,Fe)_{12}$ icosahedra, i.e., $Ga@(Cr,Fe)_{12}$, and (ii) (Cr,Fe)-centered, $[(Cr,Fe)_6Ga_6]$ icosahedra, which alternate along the *c* axis. Each of these icosahedra is surrounded by a pentagonal dodecahedron: around (i), a $[(Cr,Fe)_2Ga_{18}]$ polyhedron is

---

(25) Andersen, O. K.; Jepsen, O. *Phys. Rev. Lett.* **1984**, *53*, 2571.
(26) Andersen, O. K. *Phys. Rev.* **1975**, *B12*, 3060.
(27) Andersen, O. K.; Jepsen, O.; Glötzel, D. In *Highlights of Condensed-Matter Theory*; Bassani, F., Fumi, F., Tosi, M. P., Lambrecht, W. R. L., Eds.; North-Holland: New York, 1985.
(28) Andersen, O. K. *Phys. Rev.* **1986**, *B34*, 2439.
(29) *The Stuttgart Tight-Binding LMTO-ASA program*, version 4.7; Max-Planck-Institut für Festkörperforschung: Stuttgart, Germany, 1998.
(30) Von Barth, U.; Hedin, L. *J. Phys. C* **1972**, *5*, 1629.
(31) Koelling, D. D.; Harmon, B. N. *J. Phys. C* **1977**, *10*, 3107.
(32) Jepsen, O.; Anderson, O. K. *Z. Phys. B* **1995**, *97*, 35.
(33) Dronskowski, R.; Blöchl, P. *J. Phys. Chem.* **1993**, *97*, 8617.
(34) Blöchl, P. E.; Jepsen, O.; Andersen, O. K. *Phys. Rev.* **1994**, *B49*, 16223.
(35) Girgis, K. *Acta Crystallogr.* **1958**, *11*, 604.
(36) Häussermann, U.; Bostrøm, M.; Viklund, P.; Rapp, O.; Bjørnängen, T. *J. Solid State Chem.* **2002**, *165*, 94.
(37) Philippe, M. J.; Malaman, B.; Roques, B. *Acta Crystallogr. B* **1975**, *B31*, 477.
(38) Wells, A. F. *Structural Inorganic Chemistry*, 5th ed.; Clarendon Press: Oxford, U. K., 1984; p 1288.

Table 1. Summary of Phase Analyses for Ternary $Cr_{1-x}Fe_xGa$ Specimens by EDS, Powder XRD, and Single Crystal XRD[a]

loaded	$Cr_{0.9}Fe_{0.1}Ga$ (**1**)	$Cr_{0.8}Fe_{0.2}Ga$ (**2**)	$Cr_{0.7}Fe_{0.3}Ga$ (**3**)	$Cr_{0.6}Fe_{0.4}Ga$ (**4**)	$Cr_{0.5}Fe_{0.5}Ga$ (**5**)	$Cr_{0.4}Fe_{0.6}Ga$ (**6**)	$Cr_{0.3}Fe_{0.7}Ga$ (**7**)	$Cr_{0.2}Fe_{0.8}Ga$ (**8**)	$Cr_{0.1}Fe_{0.9}Ga$ (**9**)
					EDS				
majority	$Cr_{0.86}Fe_{0.14}Ga$	$Cr_{0.77}Fe_{0.23}Ga$	$Cr_{0.54}Fe_{0.45}Ga$	$Cr_{0.56}Fe_{0.43}Ga$	$Cr_{0.50}Fe_{0.50}Ga$	$Cr_{0.40}Fe_{0.60}Ga$	$Cr_{0.35}Fe_{0.65}Ga$	$Cr_{0.25}Fe_{0.75}Ga$	$Cr_{0.10}Fe_{0.90}Ga$
minority	$Cr_{0.60}Fe_{0.10}Ga$ $Cr_{0.25}Ga$	$Cr_{0.50}Fe_{0.17}Ga$	$Cr_{0.33}Fe_{0.33}Ga$ $Cr_{0.25}Ga$	$Cr_{0.40}Fe_{0.30}Ga$ $Cr_{0.33}Fe_{0.33}Ga$		$Cr_{0.25}Fe_{0.50}Ga$		$Cr_{0.10}Fe_{0.65}Ga$	$Cr_{0.04}Fe_{0.73}Ga$
trace							$Cr_{0.8}Fe_{1.5}Ga$	$Cr_{0.4}Fe_{1.8}Ga$	
					powder XRD				
primary	MnGa-type	MnGa-type	MnGa-type	MnGa-type	MnGa-type	MnGa-type	MnGa-type	MnGa-type	MnGa-type
secondary	Cr_3Ga-type[35]	Cr_3Ga-type[35] $FeGa_3$-type[36]	Cr_3Ga-type[35] $FeGa_3$-type[36]					Fe_3Ga_4-type[37]	Fe_3Ga_4-type[37]
					single crystal XRD				
refined	$Cr_{0.88}Fe_{0.12}Ga$	$Cr_{0.78}Fe_{0.22}Ga$	$Cr_{0.67}Fe_{0.33}Ga$	$Cr_{0.63}Fe_{0.37}Ga$	$Cr_{0.51}Fe_{0.49}Ga$	$Cr_{0.35}Fe_{0.65}Ga$	$Cr_{0.30}Fe_{0.70}Ga$	$Cr_{0.20}Fe_{0.80}Ga$	$Cr_{0.09}Fe_{0.91}Ga$
a, Å	12.6431(18)	12.6153(18)	12.5743(18)	12.5595(18)	12.5527(9)	12.5398(18)	12.5161(18)	12.4927(18)	12.4695(18)
c, Å	7.8985(16)	7.8833(16)	7.8717(16)	7.8550(16)	7.8581(13)	7.8481(16)	7.8263(16)	7.8070(16)	7.7807(16)
V, Å^3	1093.4(3)	1086.5(3)	1077.9(3)	1073.1(3)	1072.3(2)	1068.8(3)	1061.8(3)	1055.2(3)	1047.7(3)
data/params	336/29	331/30	334/29	330/29	314/29	332/29	330/29	328/29	327/29
$R\ [I > 2\sigma(I)]$	$R_1 = 0.0413$ $R_w = 0.0861$	$R_1 = 0.0708$ $R_w = 0.1283$	$R_1 = 0.0388$ $R_w = 0.0827$	$R_1 = 0.0460$ $R_w = 0.1008$	$R_1 = 0.0310$ $R_w = 0.0790$	$R_1 = 0.0430$ $R_w = 0.0897$	$R_1 = 0.0593$ $R_w = 0.1262$	$R_1 = 0.0526$ $R_w = 0.1117$	$R_1 = 0.0534$ $R_w = 0.1322$
peak/hole, e^-/Å^3	1.720/−1.578	1.725/−2.193	1.398/−1.755	1.339/−1.278	1.172/−0.942	1.382/−1.392	1.496/−1.943	1.509/−2.057	2.104/−2.003

[a] In PXRD, secondary phases are listed for each sample. For single crystal XRD results, refined lattice constants and essential statistics are included. Compositions are represented using Ga as a reference, in accord with our formulation for $Cr_{1-x}Fe_xGa$.

Table 2. Atomic Parameters and Isotropic Temperature Factors (Å^2) for the $Cr_{1-x}Fe_xGa$ Phases

atom		SOF(Cr/Fe)	*x*	*y*	*z*	U_{eq}
(**1**) $Cr_{0.88}Fe_{0.12}Ga = Cr_{11.4(1)}Fe_{1.6}Ga_{13}$						
Ga1	3*a*		0	0	0	0.012(1)
Ga2	18*h*		0.2348(1)	0.1174(1)	0.5731(2)	0.015(1)
Ga3	18*g*		0.3846(1)	3846(2)	1/2	0.014(1)
M1	3*b*	1/0	0	0	1/2	0.009(1)
M2	18*h*	1/0	0.4371(2)	0.2186(1)	0.4117(3)	0.011(1)
M3	18*h*	0.74/0.26	−0.0717(1)	0.0717(1)	0.2504(2)	0.010(1)
(**2**) $Cr_{0.78}Fe_{0.22}Ga = Cr_{10.2(1)}Fe_{2.8}Ga_{13}$						
Ga1	3*a*		0	0	0	0.013(1)
Ga2	18*h*		0.2345(2)	0.1173(1)	0.5728(3)	0.017(1)
Ga3	18*g*		0.3852(2)	0.3852(2)	1/2	0.015(1)
M1	3*b*	1/0	0	0	1/2	0.010(2)
M2	18*h*	1/0	0.4372(3)	0.2187(2)	0.4112(4)	0.012(1)
M3	18*h*	0.54/0.46	−0.0716(2)	0.0716(2)	0.2505(4)	0.012(1)
(**3**) $Cr_{0.67}Fe_{0.33}Ga = Cr_{8.7(1)}Fe_{4.3}Ga_{13}$						
Ga1	3*a*		0	0	0	0.013(1)
Ga2	18*h*		0.2337(1)	0.1168(1)	0.5740(2)	0.015(1)
Ga3	18*g*		0.3853(1)	0.3853(1)	1/2	0.013(1)
M1	3*b*	1/0	0	0	1/2	0.006(1)
M2	18*h*	0.80/0.20	0.4351(2)	0.2175(1)	0.4111(2)	0.010(1)
M3	18*h*	0.49/0.51	−0.0716(1)	0.0716(1)	0.2498(3)	0.010(1)
(**4**) $Cr_{0.63}Fe_{0.37}Ga = Cr_{8.2(1)}Fe_{4.8}Ga_{13}$						
Ga1	3*a*		0	0	0	0.015(1)
Ga2	18*h*		0.2337(2)	0.1168(1)	0.5736(2)	0.014(1)
Ga3	18*g*		0.3856(1)	0.3856(1)	1/2	0.013(1)
M1	3*b*	0.59/0.41	0	0	1/2	0.010(1)
M2	18*h*	0.60/0.40	0.4358(2)	0.2179(1)	0.4112(3)	0.012(1)
M3	18*h*	0.66/0.34	−0.0713(1)	0.0713(1)	0.2494(3)	0.010(1)
(**5**) $Cr_{0.51}Fe_{0.49}Ga = Cr_{6.6(1)}Fe_{6.4}Ga_{13}$						
Ga1	3*a*		0	0	0	0.013(1)
Ga2	18*h*		0.2334(1)	0.1167(1)	0.5742(2)	0.014(1)
Ga3	18*g*		0.3854(1)	0.3854(1)	1/2	0.013(1)
M1	3*b*	0.65/0.35	0	0	1/2	0.008(1)
M2	18*h*	0.58/0.42	0.4347(2)	0.2174(1)	0.4113(2)	0.011(1)
M3	18*h*	0.41/0.59	−0.0717(1)	0.0717(1)	0.2497(2)	0.010(1)
(**6**) $Cr_{0.35}Fe_{0.65}Ga = Cr_{4.6(1)}Fe_{8.4}Ga_{13}$						
Ga1	3*a*		0	0	0	0.015(1)
Ga2	18*h*		0.2331(1)	0.1166(1)	0.5746(2)	0.015(1)
Ga3	18*g*		0.3858(1)	0.3858(1)	1/2	0.014(1)
M1	3*b*	0.38/0.62	0	0	1/2	0.011(1)
M2	18*h*	0.49/0.51	0.4342(2)	0.2171(1)	0.4112(2)	0.013(1)
M3	18*h*	0.21/0.79	−0.0718(1)	0.0718(1)	0.2499(2)	0.013(1)
(**7**) $Cr_{0.30}Fe_{0.70}Ga = Cr_{3.9(1)}Fe_{10.1}Ga_{13}$						
Ga1	3*a*		0	0	0	0.014(1)
Ga2	18*h*		0.2329(2)	0.1164(1)	0.5747(3)	0.016(1)
Ga3	18*g*		0.3858(2)	0.3858(1)	1/2	0.015(1)
M1	3*b*	0.69/0.31	0	0	1/2	0.008(1)
M2	18*h*	0.33/0.67	0.4337(3)	0.2168(1)	0.4110(4)	0.014(1)
M3	18*h*	0.21/0.79	−0.0719(1)	0.0719(1)	0.2502(3)	0.013(1)
(**8**) $Cr_{0.20}Fe_{0.80}Ga = Cr_{2.6(1)}Fe_{10.4}Ga_{13}$						
Ga1	3*a*		0	0	0	0.015(1)
Ga2	18*h*		0.2325(2)	0.1163(1)	0.5749(3)	0.014(1)
Ga3	18*g*		0.3856(2)	0.3856(2)	1/2	0.012(1)
M1	3*b*	0/1	0	0	1/2	0.009(1)
M2	18*h*	0.26/0.74	0.4334(2)	0.2167(1)	0.4100(3)	0.011(1)
M3	18*h*	0.17/0.83	−0.0719(1)	0.0719(1)	0.2493(3)	0.011(1)
(**9**) $Cr_{0.09}Fe_{0.91}Ga = Cr_{1.2(1)}Fe_{11.8}Ga_{13}$						
Ga1	3*a*		0	0	0	0.015(1)
Ga2	18*h*		0.2321(2)	0.1161(1)	0.5754(2)	0.017(1)
Ga3	18*g*		0.3856(2)	0.3856(1)	1/2	0.015(1)
M1	3*b*	0/1	0	0	1/2	0.013(1)
M2	18*h*	0.20/0.80	0.4323(2)	0.2162(1)	0.4106(3)	0.013(1)
M3	18*h*	0/1	−0.0724(1)	0.0724(1)	0.2500(3)	0.015(1)

found; around (ii), a $[(Cr,Fe)_6Ga_{14}]$ dodecahedron occurs. With these pseudopentagonal polyhedra forming important building blocks, these structures are interesting for their relationships with icosahedral quasicrystals and their crystalline approximants.

To gain a better understanding of the distribution of Cr and Fe atoms in these phases, temperature-dependent neutron diffraction measurements on a polycrystalline sample loaded as $Cr_{0.5}Fe_{0.5}Ga$ were conducted. Figure 2 illustrates the observed and calculated neutron diffraction patterns at 295 K as an example. Figure 3 illustrates the temperature-dependent lattice constants as measured by both neutron and X-ray powder diffraction. The trends are identical, while the lattice parameters determined from the neutron data are systematically lower than those obtained from X-ray diffraction. Refinements of the neutron data, which included background coefficients, scale factors, profile functions, and absorption coefficients, as well as relaxing the site occupancies for Cr and Fe, smoothly converged to give solutions with χ_2 values, respectively, of 4.504, 4.781, and 3.694 at 11, 30, and 295 K. Additional refinements were evaluated for space groups $R\bar{3}m$ and $R\bar{3}$, neither of which resulted in significant improvements to the results. Table 3 summarizes the atomic parameters, site occupation factors, and equivalent isotropic displacement parameters for the asymmetric unit (again on the basis of the space group $R\bar{3}m$). The refined average composition of this powder sample is $Cr_{19.7(4)}Fe_{19.3(4)}Ga_{39}$ per unit cell, or $Cr_{0.505(1)}Fe_{0.495(1)}Ga$. The special position, Wyckoff site 3*b*, refines slightly richer in Cr than Fe. Among the two distinct sites building up the $(Cr,Fe)_{12}$ icosahedra centered by Ga atoms, the trigonal faces linked to the 3*b* site are richer in Fe atoms; the "waist" of the icosahedron is richer in Cr atoms. According to these refinements, these site occupancies are approximately 2/3 occupied by Cr atoms at the M2 site, and the other site connecting the adjacent icosahedra shows approximately 2/3 occupancy by Fe atoms.

An analysis of interatomic distances within $Cr_{0.505(1)}Fe_{0.495(1)}$-Ga validates the cluster-based description above. Ga1−M3 and M1−M3 distances are the shortest, ca. 2.50 Å, followed closely by M2−M3 contacts at ca. 2.58 Å and Ga1−M2 and M1−Ga2 distances at ca. 2.60 Å. Within the $Ga@(Cr,Fe)_{12}$ icosahedra, remaining distances include 2.69 Å (M3−M3), 2.75 Å (M2−M3), and 2.81 Å (M2−M2). Thus, the environment at the M2 sites gives the highest average interatomic distances among the three transition metal sites, whereas the M1 and M3 sites give lower average distances.

A neutron pair-distribution-function (PDF) analysis was also performed to investigate local structure. A combined study of Rietveld and neutron PDF analysis is generally

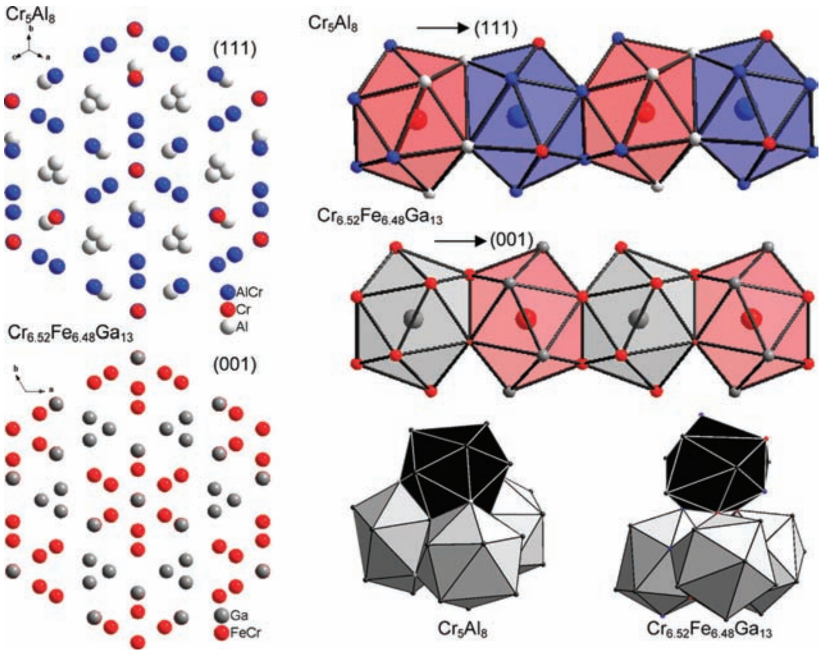

Figure 1. Structural comparison between cubic γ-brass, Cr_5Al_8, and the rhombohedrally distorted $Cr_{6.52}Fe_{6.48}Ga_{13}$. (Left) Projections of atomic positions viewed along (111) for the cubic Cr_5Al_8 γ-brass structure (top) and along (001) for the rhombohedral $Cr_{6.52}Fe_{6.48}Ga_{13}$ structure (bottom). (Right, top) One-dimensional chains of face-sharing icosahedra in Cr_5Al_8 (top) and $Cr_{6.52}Fe_{6.48}Ga_{13}$ (middle). (Bottom, right) Tetrahedra of four icosahedra in the two systems. Al and Ga atoms are white and gray spheres, respectively; the transition metals are red or blue spheres.

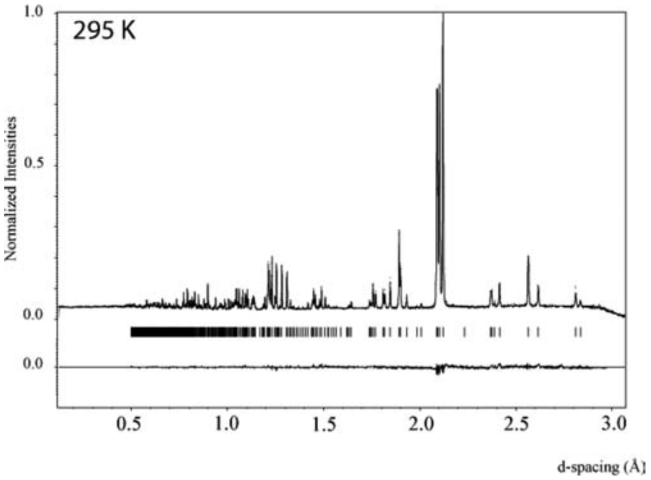

Figure 2. $Cr_{0.5}Fe_{0.5}Ga$ neutron powder pattern obtained on NPDF at 295 K. Tick marks indicate positions of the Bragg reflections. The difference between the observed and the calculated patterns is shown below the tick marks.

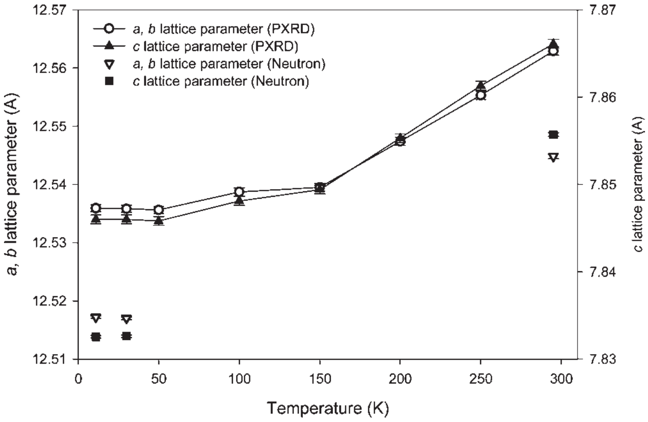

Figure 3. Nonlinear temperature dependences of the lattice parameters from powder X-ray diffraction and neutron diffraction refinement results.

helpful in providing information about the long-, medium-, and short-range ordering in a structure.[39] Indeed, Rietveld analysis determines only the average long-range structure because it only takes into account the intensity and the position of the Bragg peaks, whereas PDF analysis also includes information contained in the diffuse scattering. This additional information is very helpful for identifying the existence of any possible short-range order. Moreover, PDF analysis allows the structure to be refined at various ranges in distance r. In the case of $Cr_{0.505(1)}Fe_{0.495(1)}Ga$, we are particularly interested to know if any special local ordering is observable between Cr and Fe atoms for any length scale, as well as to distinguish between centrosymmetric or noncentrosymmetric space groups.

Neutron PDFs were corrected for background, the incident neutron spectrum, absorption, and multiple scattering and normalized using the vanadium spectrum to obtain the total scattering structure factor, $S(Q)$, using the program PDFgetN.[40] The PDF $G(r)$ was obtained from $S(Q)$ via the Fourier transform:

$$G(r) = 4\pi r[\rho(r) - \rho_0] = \frac{2}{\pi}\int_0^{Q_{\max}} Q[S(Q) - 1]\sin Qr dQ$$

where $\rho(r)$ and ρ_0, respectively, are the atomic pair number density and average number density. The data were terminated at $Q_{\max} = 40$ Å^{-1}. PDF modeling was carried out

---

(39) Proffen, T.; Billinge, S. J. L.; Egami, T.; Louca, D. *Z. Kristallogr.* **2003**, *218*, 132.

(40) Peterson, P. F.; Gutmann, M.; Proffen, Th.; Billinge, S. J. L. *J. Appl. Crystallogr.* **2000**, *33*, 1192.

Table 3. Fractional Atomic Coordinates, Site Occupation Factors, and Equivalent Isotropic Displacement Parameters for $Cr_{0.5}Fe_{0.5}Ga$ at 11, 30, and 295 K As Refined by Neutron Powder Diffraction (Rietveld Method; Space Group, $R\bar{3}m$)

sites	SOF (Cr/Fe)	x	y	z	U_{eq}
		11 K			
cell parameters		a = 12.5172(2) Å, c = 7.8325(2) Å			
refined composition		$Cr_{0.502(6)}Fe_{0.498}Ga = Cr_{6.523}Fe_{6.477}Ga_{13}$			
Ga1 (3*a*)		0	0	0	0.0051(1)
Ga2 (18*h*)		0.23328(4)	0.11664(2)	0.57472(5)	0.00448(7)
Ga3 (18*g*)		0.38580(3)	0.38580(3)	1/2	0.00412(7)
M1 (3*b*)	0.577(5)/0.423	0	0	1/2	0.00247(6)
M2 (18*h*)	0.625(2)/0.375	0.43369(4)	0.21684(2)	0.41218(6)	0.00363(6)
M3 (18*h*)	0.366(3)/0.634	−0.07156(2)	0.07156(2)	0.24985(6)	0.00407(6)
		30 K			
cell parameters		a = 12.5170(2) Å, c = 7.8326(2) Å			
refined composition		$Cr_{0.502(6)}Fe_{0.498}Ga = Cr_{6.523}Fe_{6.477}Ga_{13}$			
Ga1 (3*a*)		0	0	0	0.0051(1)
Ga2 (18*h*)		0.23327(4)	0.11664(2)	0.57471(5)	0.00459(7)
Ga3 (18*g*)		0.38576(3)	0.38576(3)	1/2	0.00414(7)
M1 (3*b*)	0.568(5)/0.432	0	0	1/2	0.00288(8)
M2 (18*h*)	0.627(2)/0.373	0.43370(4)	0.21685(2)	0.41221(6)	0.00365(8)
M3 (18*h*)	0.366(3)/0.634	−0.07156(2)	0.07156(2)	0.24989(6)	0.00402(8)
		295 K			
cell parameters		a = 12.5448(4) Å, c = 7.8557(2) Å			
refined composition		$Cr_{0.515(10)}Fe_{0.485}Ga = Cr_{6.701}Fe_{6.299}Ga_{13}$			
Ga1 (3*a*)		0	0	0	0.0096(2)
Ga2 (18*h*)		0.23302(5)	0.11651(3)	0.57462(8)	0.0117(2)
Ga3 (18*g*)		0.38530(3)	0.38530(3)	1/2	0.0101(1)
M1 (3*b*)	0.587(9)/0.413	0	0	1/2	0.0054(3)
M2 (18*h*)	0.636(1)/0.364	0.43380(7)	0.21690(2)	0.41118(3)	0.0072(2)
M3 (18*h*)	0.383(5)/0.617	−0.07154(7)	0.07154(7)	0.24971(2)	0.0074(1)

using the program PDFGUI[41] by using the results obtained from the Rietveld refinement as the starting structural model. First, we relaxed numerous symmetry constraints, but no significant improvements were observed, a result which indicates that the centrosymmetric space group $R\bar{3}m$ is the best choice to describe the average structure. Second, a total relaxation was investigated to model possible short-range ordering within the network of Cr and Fe sites, e.g., local domains of Cr or Fe atoms as "islands" or "strips." As presented in Figure 4, the fit is impressively good up to r = 40 Å, which implies that no disorder is observable at least up to that length scale. Therefore, neutron PDF analysis indicates that the local structure and the average structure obtained from Rietveld refinement are quite similar and no visible disorder is observed.

Magnetic Behavior of $Cr_{0.5}Fe_{0.5}Ga$. According to our phase analysis using EDS and powder XRD, only the loaded sample $Cr_{0.5}Fe_{0.5}Ga$ produced a single-phase product, $Cr_{0.505(1)}Fe_{0.495(1)}Ga$, within the errors allowed by both techniques. Thus, magnetic susceptibility measurements were limited to this sample. Figure 5 illustrates the magnetic susceptibility measured at a 1 kOe external field. Above 125 K, the linear behavior suggests Curie−Weiss behavior with an effective magnetic moment of ca. 4.2 μ_B per formula unit. Extrapolating the linear curve yields a Weiss temperature of ca. −15 K. Below 24 K, the inverse magnetic susceptibility shows an upturn, probably related to antiferromagnetic order. The upper inset in Figure 5 shows the low-temperature field-cooled and zero field-cooled susceptibility data below 30 K. The higher temperature slope change (ca. 24 K) in magnetic susceptibility shows no difference between field and zero-field cooled data, whereas magnetic susceptibility manifests with clear hysteresis below 16 K. The magnetization isotherms, $M(H)$, at 2 K are plotted in the lower insets of Figure 5; a small hysteresis below 30 kOe was observed with metamagnetic-like behavior.

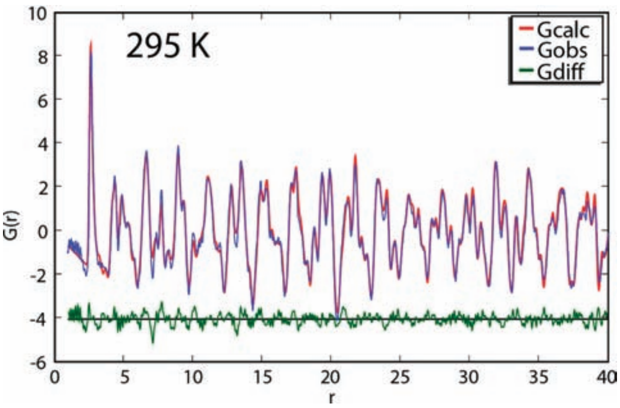

Figure 4. PDF refinement over the r_{min} (1.0 Å) to r_{max} (40.0 Å) range for $Cr_{0.5}Fe_{0.5}Ga$. The red, blue, and green curves correspond to the $G(r)$ calculated and observed and the difference, respectively.

The variation of the lattice parameters with temperature, as observed by both neutron and X-ray powder diffraction, shows nonlinear behavior at lower temperatures. The high temperature, paramagnetic phase exhibits a larger volume, through expanded lattice constants, than the extrapolation of the low temperature lattice constants to higher temperatures. Thus, we see the existence of magnetostriction.[42] This

---

(41) Proffen, Th.; Billinge, S. J. L. *J. Appl. Crystallogr.* **1999**, *32*, 572–575.

(42) du Tremolet de Lacheisserie, E. *Magnetostriction: Theory and Applications of Magnetoelasticity*; CRC Press: Boca Raton, FL, 1993.

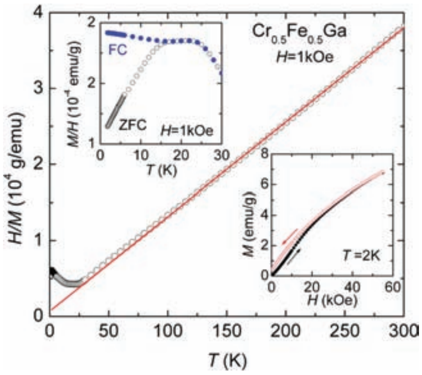

Figure 5. Magnetic susceptibility measured on powder samples of $Cr_{0.5}Fe_{0.5}Ga$.

is further confirmed by looking at the reflections in real space rather than in reciprocal space obtained by Fourier transformation of the raw neutron powder diffraction data to generate the pair distribution function (PDF, $Q(r)$).[41]

Relationship to γ-Brasses. The rhombohedral structures of $Cr_{1-x}Fe_xGa$ are closely related to the cubic γ-brass structure and are isostructural with many rhombohedrally distorted Cr_5Al_8-type structures found in the Al−Cr, Al−Cu, Ga−Cr, Ga−Mn, and Ga−Fe systems.[15,18] All structures share the fundamental building block of four tetrahedrally fused icosahedra, which are illustrated in Figure 1. In the cubic γ-brass structure, four icosahedra construct a perfect tetrahedron by sharing faces, but in the rhombohedrally distorted structure, three icosahedra share faces with one sitting on top of the other three sharing only edges.

Another description of cubic γ-brass structures utilizes a body-centered cubic packing of 26-atom clusters formed by the following "shells" of atoms: (i) an inner tetrahedron, (ii) an outer tetrahedron of sites capping each face of the inner tetrahedron, (iii) an octahedron sitting over each edge of the outer tetrahedron, and (iv) a distorted cuboctahedron. A recent investigation of $Cu_{5\pm x}Zn_{8\mp x}$, which combined neutron powder diffraction with electronic structure theory, demonstrated that the inner tetrahedron is always fully occupied by Zn atoms, the outer tetrahedron is always fully occupied by Cu atoms, and the range in composition occurs by subsequent statistical occupation by Cu and Zn atoms in the octahedron and cuboctahedron.[6] The structures of $Cr_{1-x}Fe_xGa$ resemble this pattern: (i) The inner tetrahedron is formed by the transition metals Cr and Fe (M1 + 3 M3 sites). (ii) The outer tetrahedron is exclusively formed by Ga atoms (Ga1 + 3 Ga2 sites). (iii) The octahedron involves three transition metals and three Ga atoms (3 Ga2 + 3 M2 sites). (iv) The cuboctahedron contains six transition metals and six Ga atoms (6 Ga3 + 3 M2 + 3 M3 sites). Thus, the two inner tetrahedra form a kernel, $[M_4Ga_4]$, while the outer octahedron and cuboctahedron provide a 3D template in which these clusters are encapsulated. This template shows mixed site occupancies in either an ordered (as in $Cr_xFe_{1-x}Ga$) or disordered (as in $Cu_{5\pm x}Zn_{8\mp x}$) manner.

The unit cell of these rhombohedral $Cr_{1-x}Fe_xGa$ structures, when transformed to include the two distorted 26-atom γ-brass related clusters, are slightly distorted away from cubic metrics with angles ranging from 89.15 to 89.27°. Pearson et al. have suggested that the rhombohedral distortion of the cubic γ-brass structure occurs as a result of the band structure energy stabilization when the number of conduction electrons per 52-atom unit cell increases from the range ca. 84−90 electrons to values of ca. 95−100 electrons.[18] In this formalism, only valence s and p electrons are counted, and not valence d electrons. The contribution from the transition metals to the number of conduction electrons is often confusing in this context: in some counting schemes, Cr and Fe would contribute no conduction electrons; in others, they would be counted as one electron.[43,44] There are even arguments that the transition metal d band will reduce the number of conduction electrons.[44] Nevertheless, the total valence electron counts for the cubic and rhombohedral cases differ significantly: if we include all valence d electrons, including the 3d core electrons for the post-transition element Ga, then the valence electron count for the $Cr_{1-x}Fe_xGa$ series would range from 9.5 to 10.5 spd electrons per atom, while the cubic γ-brasses would require ca. 11.6 spd electrons per atom. Nevertheless, on the basis of the phases showing rhombohedral distortions, the Fermi level will fall among valence d orbitals of the transition metal, whereas the γ-brasses show the valence d bands to be somewhat below the Fermi level.

To explore Pearson's conjecture[18] quantitatively, we have integrated the s and p portions of the total DOS curves for cubic Cu_5Zn_8[6] and rhombohedral CrGa and FeGa.[15] In these specific cases, the cubic γ-brass integrates to 1.78 sp e^-/atom (93 electrons per 52 atom cell); the rhombohedral cases give ca. 2.00 sp e^-/atom (104 electrons per 52 atom cell). Further computational investigations are underway to examine possible driving forces within the electronic structure for this structural effect among γ-brass related phases.

Theoretical Electronic Structures. The theoretical electronic structures of various models from the $Cr_{1-x}Fe_xGa$ series were determined and analyzed to assess the trends in the distribution of Cr and Fe atoms in the structure, which we call the "coloring problem,"[45] and to shed some light on the magnetic character of $Cr_{0.5}Fe_{0.5}Ga$. Since this system represents a complex computational problem, only specific preliminary results will be related; a broader computational study is underway.

Coloring Problem. According to the refinement of site occupancies in $Cr_{0.5}Fe_{0.5}Ga$ by neutron diffraction, the distribution of Cr and Fe atoms is neither completely random nor completely ordered. Cr atoms prefer the M2 sites, which form the waist of the Ga-centered $(Cr,Fe)_{12}$ icosahedron, and the M1 sites, which bridge adjacent icosahedral clusters along the *c* direction. Likewise, Fe atoms prefer the M3 sites, which form the upper and lower triangles of the $(Cr,Fe)_{12}$ icosahedron. Perusal of the refinement results in Table 2 from the nine samples of the $Cr_{1-x}Fe_xGa$ series studied by single crystal XRD shows a qualitatively similar trend to the one seen in $Cr_{0.5}Fe_{0.5}Ga$ with a few amendments based on the range of chemical composition covered by the series. First, Fe atoms generally prefer to occupy the M3 sites throughout

---

(43) Barrett, C.; Massalski, T. B. *Structure of Metals*, 3rd ed.; Pergamon Press: New York, 1980.

(44) Watson, R. E.; Bennett, L. H. *Phys. Rev. B* **1978**, *18*, 6439.

(45) Miller, G. J. *Eur. J. Inorg. Chem.* **1998**, 523.

the series (the only exception is sample **4**), and Cr atoms prefer to occupy the M2 sites. Second, Cr atoms fill the bridging M1 sites for a low Fe content, whereas these M1 sites refine as completely occupied by Fe atoms at a high Fe content.

A tight-binding analysis of the total electronic energy has suggested that there are two factors influencing the distribution of elements in an intermetallic structure: (i) a *site-energy* term and (ii) a *bond-energy* term.[18] In many inorganic solids, one of these two terms tends to dominate. For example, ionic solids, which show the highest electronegativity differences between component elements, optimize the *site-energy* term through a distribution that minimizes the Madelung potential. On the other hand, elemental solids optimize the *bond-energy* term. Intermetallic compounds often show results that represent the best compromise between these two different factors.[46] In such compounds, a Mulliken population analysis[47] can quickly assess the arrangement that minimizes the *site-energy* term: sites with higher Mulliken populations attract the metallic element with lower valence atomic orbital energies. Thus, for the $Cr_{1-x}Fe_xGa$ series, an extended Hückel calculation on MGa (= $M_{13}Ga_{13}$; M = Mn atomic parameters; structural parameters from results of neutron powder diffraction at 11 K for $Cr_{0.5}Fe_{0.5}Ga$) with the valence electron count allowed to vary from 9.0 e^- (M = Cr) to 11.0 e^- (M = Fe) per MGa unit indicated the preference for Fe occupation on the basis of the *site-energy* term followed M2 > M3 ≫ M1. Thus, there is a considerable contribution from the *bond-energy* term, i.e., interatomic orbital interactions, influencing the distribution of Cr and Fe atoms, an effect which is also reflected in the interatomic distances.

To examine this conclusion semiquantitatively, the total energies of various models of the mixed-metal systems $Cr_{13-n}Fe_nGa_{13}$, $0 < n < 13$, using TB-LMTO calculations are compared against the corresponding mixtures of $Cr_{13}Ga_{13}$ and $Fe_{13}Ga_{13}$. Figure 6 illustrates the trend in these relative energies, which can be expressed as

$$\Delta E^{(i)}(n) = [E^{(i)}(n) - E^{(1)}(0)] - \frac{n}{13}[E^{(i)}(13) - E^{(1)}(0)]$$

where $E^{(i)}(n)$ is the averaged total energy of $Cr_{13-n}Fe_nGa_{13}$ for Fe atoms occupying M*i* sites (*i* = 1, 2, and 3, according to Tables 2 and 3) as fully as possible. Therefore, $E^{(1)}(0)$ and $E^{(1)}(13)$ are the total energies, respectively, of $Cr_{13}Ga_{13}$ and $Fe_{13}Ga_{13}$. In Figure 6, the different shapes of the data points represent the different sites (circle = M1; square = M2; triangle = M3); the colors correspond to Fe or Cr (red = Fe; blue = Cr). The lines connect the averaged total energies for Fe or Cr in the M1 (3*b*) sites. The overall trend in these energy differences shows the effect of different third moments of the electronic DOS on the relative total energies.[48] According to this moments argument, the weighted average of the third moments of the DOS of $Cr_{13}Ga_{13}$ and $Fe_{13}Ga_{13}$ will be higher than the third moments of mixed metal $Cr_{13-n}Fe_nGa_{13}$. The third moment is a measure of the skewness of the DOS function and indicates the differences in three-membered rings in the different structures, i.e., rings which represent a sequence of atoms connected to each other by valence orbital overlap. Conclusions from this computational analysis of the averaged total electronic energies include the following: (1) Cr prefers to occupy the M1 site for all compositions. (2) For a low Fe content, Fe slightly prefers the M3 sites but shows an energetic preference for the M2 sites at a high Fe content. (3) The energy differences between different colorings range from 40 to 50 meV per $Cr_{13-n}Fe_nGa_{13}$. These energy differences are small with respect to the temperature scale of preparation (50 meV ~ 600 K), so entropy effects will play a significant role in the observed elemental distributions. Configurational entropy alone, which is at a maximum for $x = 0.5$ in $Cr_{1-x}Fe_xGa$, will account for ca. 40 meV per formula unit at 600 K. Some general trends, e.g., Cr atom preference for the M1 site and Fe atom preference for the M3 site, are consistent, in part, with the experimental findings.

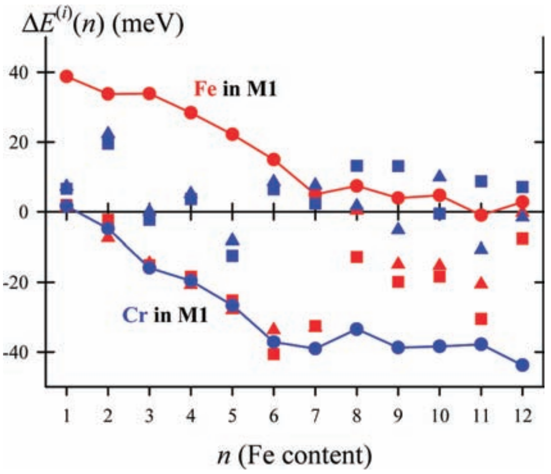

Figure 6. Relative total energies between models for $Cr_{13-n}Fe_nGa_{13}$ and the corresponding mixture of $Cr_{13}Ga_{13}$ and $Fe_{13}Ga_{13}$ according to the equation described in the text. Red data points focus on Fe atoms; blue data points focus on Cr atoms. Circles = M1 sites exclusively occupied. Squares = M2 sites exclusively occupied. Triangles = M3 sites exclusively occupied. Lines connect relative energies for Fe (red) or Cr (blue) exclusively occupying the M1 sites.

Electronic Structure of "$Cr_{0.5}Fe_{0.5}Ga$". Spin-polarized TB-LMTO-ASA band calculations were performed on four model structures to investigate features of its electronic structure and to elucidate possible magnetic structures of "$Cr_{0.5}Fe_{0.5}Ga$". Given that there are an odd number of transition metals per primitive unit cell, two distinct compositions were examined: "$Cr_7Fe_6Ga_{13}$" and "$Cr_6Fe_7Ga_{13}$". In "$Cr_7Fe_6Ga_{13}$," the M1 (3*b*) site is occupied by Cr atoms, and two different models placed the remaining Cr atoms on either the M2 or M3 sites. Likewise, in "$Cr_6Fe_7Ga_{13}$," the M1 (3*b*) site is occupied by Fe atoms, and two different models placed the remaining Fe atoms on either the M2 or M3 sites. Table 4 lists the band energies, given relative to the lowest energy case for each composition, total magnetic moment, and atomic populations and local atomic moments for each crystallographic site. The local atomic moments, μ, are also identified with a sign, which signifies whether the local electron densities integrate toward excess "spin-up" (+)

---

[46] Miller, G. J.; Lee, C.-S.; Choe, W. *Highlights in Inorganic Chemistry*; Meyer, G., Ed.; Wiley-VCH: New York, 2002; p 21.

[47] Burdett, J. K. *Chemical Bonding in Solids*; Oxford University Press: New York, 1995.

[48] Hoistad, L. M.; Lee, S. *J. Am. Chem. Soc.* **1991**, *113*, 8216.

Table 4. Results from TB-LMTO-ASA Calculations on Ordered Model Structures for $Cr_7Fe_6Ga_{13}$ and $Cr_6Fe_7Ga_{13}$[a]

		$Cr(Cr_6Fe_6)Ga_{13}$						$Fe(Cr_6Fe_6)Ga_{13}$				
E_{band}(LSDA)		0.000 eV			1.921 eV			0.000 eV			2.416 eV	
μ_{tot}		2.419 μ_B			4.618 μ_B			9.769 μ_B			11.050 μ_B	
E_{band}(LDA)		0.079 eV			2.085 eV			0.536 eV			2.517 eV	
		Q	μ		Q	μ		Q	μ		Q	μ
Ga1 (3*a*)		2.94	+0.01		3.04	+0.01		2.97	+0.02		3.04	+0.01
Ga2 (18*h*)		2.89	+0.00		2.90	+0.03		2.88	+0.01		2.88	+0.02
Ga3 (18*g*)		3.11	+0.00		3.01	+0.05		3.11	+0.02		3.01	+0.05
M1 (3*b*)	Cr:	5.91	+0.17	Cr:	6.25	+0.05	Fe:	8.12	−2.33	Fe:	8.45	−1.80
M2 (18*h*)	Cr:	5.86	+0.16	Fe:	8.19	−1.07	Cr:	5.88	+0.35	Fe:	8.21	−0.95
M3 (18*h*)	Fe:	8.16	−0.59	Cr:	5.85	+0.21	Fe:	8.11	−1.62	Cr:	5.82	−0.66

[a] Electronic band energies (relative to the lower energy model for both LDA and LSDA approaches), total magnetic moments (in μ_B), and local magnetic moments (μ) and valence electron populations (Q) are listed. The different models reflect different colorings of the transition metal sites.

or “spin-down” (−) electrons. For both compositions, the lower energy model gives the lower total magnetic moment, showing local ferrimagnetic ordering at the transition metals along the *c* direction; the local moments at the transition metal sites do not all have the same sign, as in ferromagnetic ordering, nor do they completely compensate each other. Local moments at the Ga atom sites are ca. 0 μ_B. When Cr occupies the M1 site, which links two Ga@M_{12} icosahedra, the near-neighbor exchange coupling along the *c* direction is antiferromagnetic. On the other hand, when Fe occupies the M1 site, the near-neighbor Fe−Fe exchange coupling (Fe1−Fe3) is ferromagnetic (local moments have the same sign in Table 4), whereas the Cr−Fe exchange coupling is antiferromagnetic (local moments have the opposite sign in Table 4). Thus, in both cases, the exchange coupling within the Ga@M_{12} icosahedral cluster is antiferromagnetic, but the exchange coupling between the cluster and the bridging atom depends on the identity of the bridge site: ferromagnetic if Fe, antiferromagnetic if Cr. In MnGa,[14] two magnetic models converged. The lower energy model gave a large total magnetic moment (25.24 μ_B/cell), with ferromagnetic coupling within the Ga@Mn_{12} icosahedron and antiferromagnetic coupling between the bridging atom (M1 site) and the cluster. The second possible magnetic structure, which was 0.24 eV/cell higher in energy, resembled the preferred magnetic model of “$Cr_7Fe_6Ga_{13}$”.

The DOS and selected COHP curves of the lower energy models of “$Cr_7Fe_6Ga_{13}$” and “$Cr_6Fe_7Ga_{13}$” are illustrated in Figure 7 for a narrow energy region around the calculated Fermi levels. These DOS curves show three distinct features: (i) There is a long tail of low DOS values extending to low energies beginning at ca. 2 eV below the Fermi levels. (ii) A transition metal 3d band, arising mostly from the icosahedral cluster, Ga@$(Cr,Fe)_{12}$, that is ca. 4 eV wide, straddles the Fermi level and has a two-peak appearance indicative of the metal icosahedron.[14,15] (iii) The Fermi levels fall at a deep, narrow pseudogap. The low-energy tails arise primarily from the 4s and 4p valence orbitals of Ga atoms mixing with the transition metal 4s and 3d levels; the valence sp band extends over all valence energies, as shown by the gray-shaded regions. These two DOS curves also exhibit two subtle differences: (i) The partial DOSs from orbitals at the M1 site, Cr in “$Cr_7Fe_6Ga_{13}$” and Fe in “$Cr_6Fe_7Ga_{13}$,” reflect the small electronegativity difference between Cr and Fe. (ii) The majority and minority spin DOS curves show slight differences for “$Cr_7Fe_6Ga_{13}$” and greater differences for “$Cr_6Fe_7Ga_{13}$”. For “$Cr_7Fe_6Ga_{13}$,” orbitals from the Cr1 site have greater contributions to states above the Fermi level (see black regions) than below. In “$Cr_6Fe_7Ga_{13}$,” orbitals from the Fe1 site show a significant contribution ca. 1.5 eV below the Fermi level, but also over a 1 eV range above the Fermi level (see also black regions in the DOS curve). The small differences in majority and minority spin DOS curves of “$Cr_7Fe_6Ga_{13}$” reflect the small local magnetic moments calculated at the Cr sites (see Table 4): 0.16 and 0.17 μ_B. Larger local moments at Fe atom sites become evident in “$Cr_6Fe_7Ga_{13}$”.

In Figure 7, crystal orbital Hamilton population (COHP) curves[33] are also shown for M−M interactions, viz., M1−(M2,M3) and (M2,M3)−(M2,M3) contacts. In the Cr-rich “$Cr_7Fe_6Ga_{13}$,” these orbital interactions are nearly optimized, the Fermi level lies just into weakly antibonding orbitals. For the Fe-rich “$Cr_6Fe_7Ga_{13}$,” intraicosahedral interactions remain similar, but the Fermi level lies deeper into antibonding Fe1−(Cr,Fe) interactions, which is consistent with the ferromagnetic Fe1−Fe3 coupling in this model.[49,50] The (Cr,Fe)−Ga interactions, whose COHP curves are not illustrated, do not reveal a crossover between bonding and antibonding states near the Fermi level and, thus, are insignificant for the subtle structural and magnetic behavior of these phases. These interactions, nonetheless, are important for the gross cohesive energies.

Certainly, further theoretical investigations are warranted to fully characterize this complex system. In general, however, the intrinsic heteroatomic orbital interactions induce a significant decrease in splitting between the two spin states at both Cr and Fe sites in $Cr_{1-x}Fe_xGa$, which further results in a shift of the Fermi level toward the crossover point between bonding and antibonding interactions in the Cr-rich case, and significant modification of local magnetic moments from homonuclear cases. This effect has been observed, in part, in theoretical calculations on ordered body-centered cubic models of Cr−Fe alloys; e.g., in CsCl-type “CrFe,” the calculated moments are 1.10 μ_B at Fe and 0.68 μ_B at Cr, as compared to 2.19 μ_B for bcc-Fe and 0.18 μ_B for bcc-Cr.[51] In this example, the moment at Fe is greatly reduced, whereas the moment at

---

(49) Dronskowski, R.; Landrum, G. *Angew. Chem., Int. Ed. Engl.* **2000**, *39*, 1560.

(50) Samolyuk, G.; Miller, G. J. *J. Comput. Chem.* **2008**, *29*, 2177.

(51) Moroni, E. G.; Jarlborg, T. *Phys. Rev. B* **1993**, *B47*, 3255.

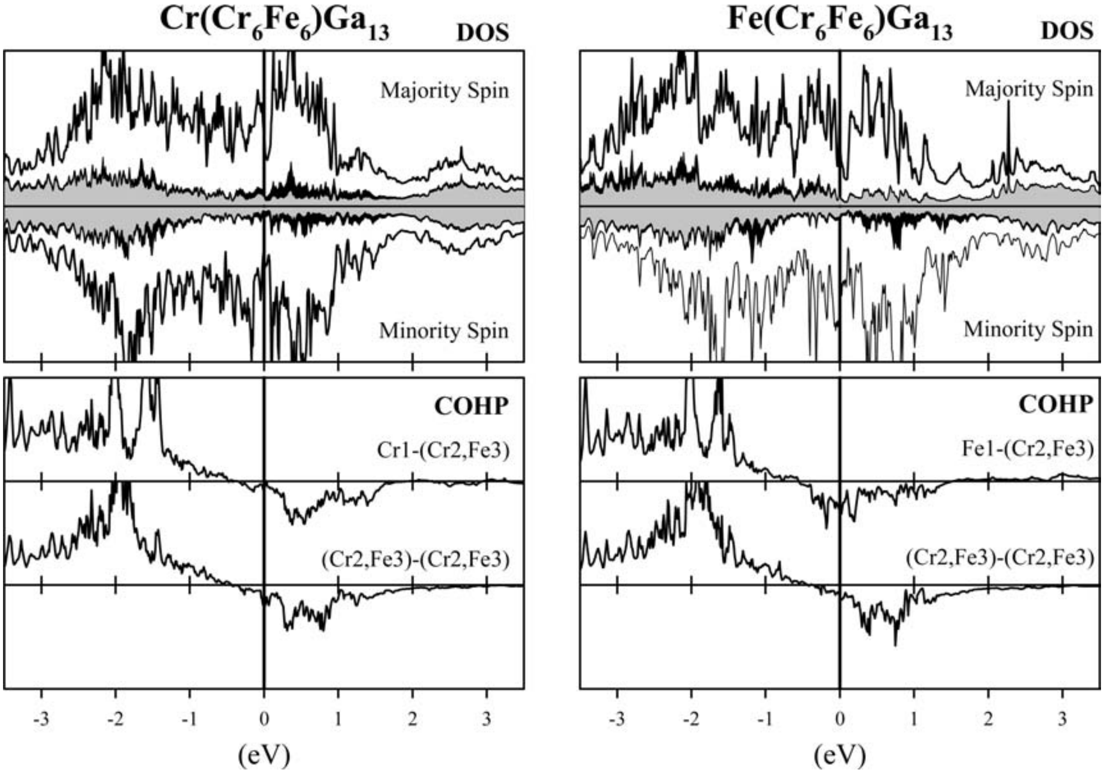

Figure 7. (Top) Total DOS curves for (left) $Cr_7Fe_6Ga_{13}$ and (right) $Cr_6Fe_7Ga_{13}$, separated into majority and minority spin states. Black regions are projections of orbitals from the M1 sites; gray regions are sp orbitals. (Bottom) COHP curves for M1−(M2, M3) and (M2, M3)−(M2, M3) contacts. The corresponding Fermi levels are marked by the thick solid line.

Cr is enhanced as compared to the elements themselves. Our results for "$Cr_7Fe_6Ga_{13}$" and "$Cr_6Fe_7Ga_{13}$," however, reveal lower moments for both Cr and Fe sites when compared to the binary cases CrGa and FeGa.

Conclusions

The rhombohedral $Cr_{1-x}Fe_x$ Ga structures have similar crystal structural features with cubic γ-brasses and specifically exhibit one-dimensional chains of face-sharing icosahedra isolated by the surrounding Ga atoms. As shown in Figure 1, trigonal distortion occurs in the $Cr_{1-x}Fe_x$ Ga series from the cubic γ-brass structure via shift of one icosahedron from the tetrahedrally stacked cluster of four icosahedra. Furthermore, the distribution of Cr and Fe atoms, as refined from neutron diffraction patterns, is not entirely random, a distribution that represents a compromise between site-energy and bond-energy forces. Although isostructural with previously studied binaries CrGa,[15] MnGa,[14] and FeGa[15] with significant atomic magnetic moments (ca. 0.7−1.3 μ_B for Cr, ca. 2.0−2.6 μ_B for Mn, and ca. 1.7−2.2 μ_B for Fe), the ternary models "$Cr_7Fe_6Ga_{13}$" and "$Cr_6Fe_7Ga_{13}$" both gave ferrimagnetic structures with significantly lower local magnetic moments. The total magnetization values, based on interatomic exchange coupling, were also low. Both of these theoretical results arise from heteroatomic Cr−Fe orbital interactions, which tend to decrease the magnitudes of local magnetic moments in itinerant magnets, as seen along the isoelectronic sequence bcc-Cr, VMn, and TiFe, which is Pauli paramagnetic.[52] Finally, band structure calculations indicated the existence of a pseudogap near the Fermi energy, the origin of which remains elusive. Further theoretical examination of these and similar systems will explore the effect of atomic colorings and structural distortions on this pseudogap in the DOS curves.

Acknowledgment. This work was carried out at the Ames Laboratory, which is operated for the U.S. Department of Energy by Iowa State University under Contract No. DE-AC02-07CH11358. This work was supported by the Materials Sciences Division of the Office of Basic Energy Sciences of the U.S. Department of Energy.

Supporting Information Available: Crystallographic files of the structures described in this work. This material is available free of charge via the Internet at http://pubs.acs.org.

---

(52) Gourdon, O.; Gout, D.; Miller, G. J. In *Encyclopedia of Condensed Matter Physics*; Bassani, G., Liedl, G., Wyder, P., Eds.; Elsevier: Amsterdam, 2005; pp 409−422.